Journal of Mechanical Systems for Transportation and Logistics

Vol. 1, No. 1, 2008

Aerial Robotic System for Transportation and Logistics*

Kakuya IWATA**, Naohisa HASHIMOTO** and Kiyoshi KOMORIYA**

**National Institute of Advanced Industrial Science and Technology (AIST),

1-2-1, Namiki, Tsukuba, Ibaraki, Japan

E-mail: k.iwata@aist.go.jp

Abstract

The status quo of a research on a novel aerial robotic system for transportation and logistics is presented. Under a new concept for an aerial robotic transportation system, three-Dimensional Transportation Robots (3DTR) were constructed with twin turbojet engines equipped by high performance noise reduction system and a flexibly jointed delta wing controlled by 2-axis actuators. This vehicle is also stable in the air due to its pendulum structure. The first flight was successfully conducted on November 22, 2005. Flight examination of 3DTR indicates its short take-off and landing (STOL) capability.

Key words: Aerial Transportation Robotics, Aerial Robotic Network for Transportation and Logistics

1. Introduction

This research is a challenge for creation of a novel personal transportation system. Transportation is indispensable not only for various industry sectors but also daily personal life. Transportation systems can be classified into two types, public and personal ones as shown in Table 1. The Important point is differences of production scales. Markets for personal have become larger than that for public in history, because the former one matches mass production. Progresses in transportation systems have been made from hub-spoke styles to random point-to-point traffics and air traffic is suitable for random point-to-point transportation system due to its large capacity of 3-dimensional space. However, in the air, personal vehicles for point-to-point traffic are not yet freely available. This is why we are trying to develop a newly conceived 3-dimensional transportation robot (3DTR). An aerial robotic system for transportation and logistics is one application of the 3DTR.

Table. 1 Comparison between typical public and personal transportation systems

Item	Surface		Air	
	Public	Personal	Public	Personal
Vehicle Type	Train	Automobile	Air line	3DTR
Door to Door	Unable	Able	Unable	Able
Speed	Fast	Slow	Fast	Slow
No. of Passengers	Many	Few	Many	Few
Life Time	Long	Short	Long	Short
Vehicle Price	High	Low	High	Low
Production Mass	Few	Many	Few	Many
Industrial Scale	Smaller	Larger	Smaller	Larger

*Received 6 Sep., 2007 (No. 07-0514)
[DOI: 10.1299/jmtl.1.146]

Table 1 indicates that the travel speed of 3DTR could be much slower compared with airline transporters. This is analogous to a comparison between train and automobile as shown in Table 1. This difference of traveling speed is most important and makes the starting point of this research. Table 1 indicates that high speed unnecessary for personal use. Figure 1 shows a matured 3DTR system image for the future. This system consists of slow speed 3DTRs and high-speed ground-based manipulation robots that are able to catch and launch 3DTRs.

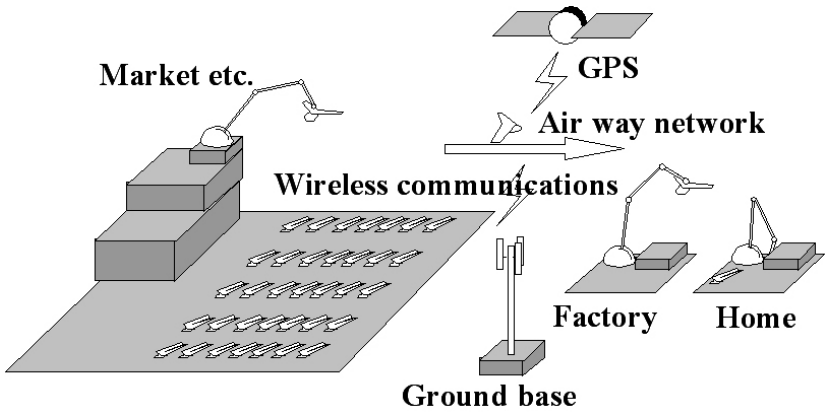

Fig.1 Concept of a novel personal air transportation system.

Technological realizations of slow speed 3DTR and high-speed manipulation of ground-based take-off and landing bring this system real. This kind of a large ground-based manipulation robot is commercially available by a Japanese foremost machine builder as shown in Fig.2.

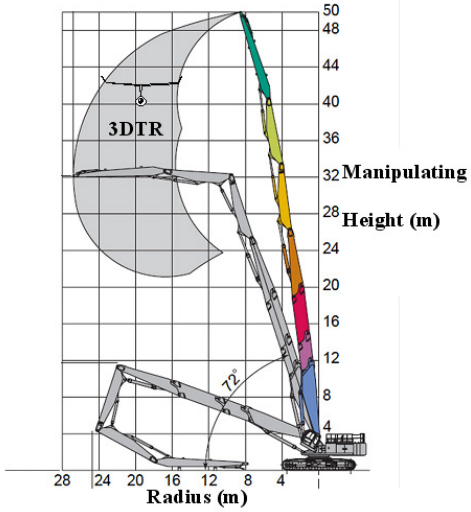

Fig. 2 A high-speed ground-based manipulation robot.

This machine can swing its arm tip up to 40km/h. Its speed seems high enough to catch a 3DTR at a slow flight speed. So, the first objectives of this research are to make a 3DTR fly safely at this slow speed of below 40km/h.

Traffic control system is also important to bring this Fig.1 system real. Traffic should be controlled by network system and tracking technique of individual aerial robots. Research

of tracking of aerial robot had been reported for helicopter,[1,2] fixed wing small airplane, [3] and airship[4,5] since middle of 1990's. These autonomous tracking technologies of aerial robot will be applied for this air transportation system of Fig.1.[6]

2. Concept and basic design of 3DTR

Stability in slow flights is indispensable for a 3DTR, and at the same time gust alleviation features are required. Figure 3 shows a structure and a pendulum attitude stability method of 3DTR, which enable to absorb both rotational and translation shocks by gusts.

A wing weight of 3DTR must be as light as possible in order to position the center of gravity (CG) lower to acquire pendulum effects. A fabric-covered wing is suitable for a wing of 3DTR. The wing is made of CFRP or duralumin frames and covered by synthetic fiber textile, then it can be folded easily during parking on the ground as shown in Fig.4. The lightweight flexible wing is connected to the dangling body at a single point near the center of MAC (mean aerodynamic chord) with an actuator-controlled joint. Reducing stall velocity and attitude controllability at slow flight speed could be respectively attained by small wing loading and the CG control method. The actuator-controlled joint driven by roll- and pitch-axis servomotors can shift CG and steer 3DTR.

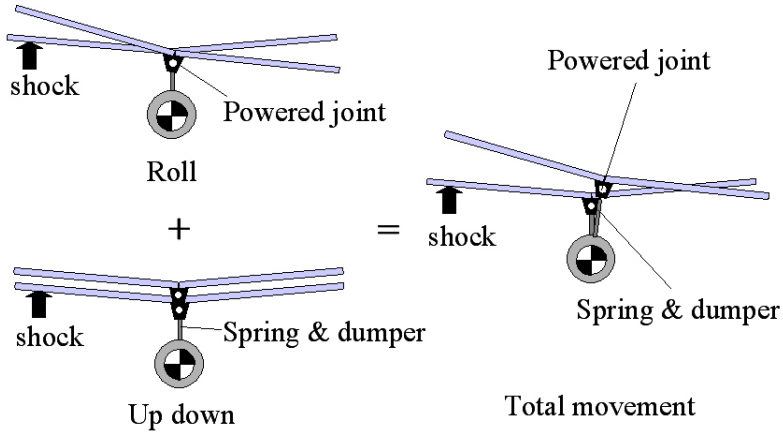

Fig. 3 The basic structure of 3DTR.

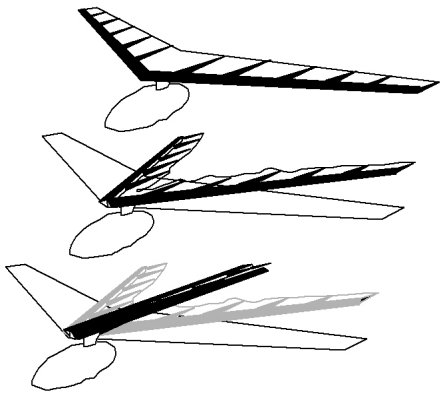

Fig. 4 Foldable flexible wing of 3DTR.

This 3DTR structure makes its design work easy and simple. Only by measuring L/D (lift/drag) ratios of the wing and drag of the body, the required thrust of 3DTR could be calculated as shown in Fig.5.

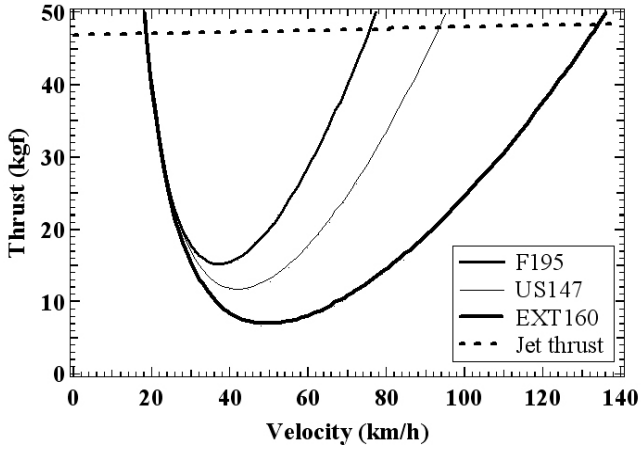

Fig. 5 Required thrusts of three flexible wing type and turbojet engine thrust vs. velocity.

Required thrusts are given by measured L/D values as the following;

$$D = C_D \frac{1}{2}\rho v^2 S = T_r \tag{1}$$

$$L = C_L \frac{1}{2}\rho v^2 S = W \tag{2}$$

where D, L, T_r, W, ρ, v, S, C_D and C_L are, respectively, drag, lift, required thrust, vehicle weight, air density of ISA (International Standard Atmosphere), velocity, wing area, drag coefficient and lift coefficient.

Using Eq.(1) and (2), T_r can be written as;

$$T_r = \frac{W}{C_L/C_D} = \frac{C_{D\min}}{C_L}W + \frac{C_L}{\pi eA}W = \frac{C_{D\min}S\rho}{2}v^2 + \frac{2W^2}{\pi eAS\rho}\frac{1}{v^2} \tag{3}$$

where A, e, and C_{Dmin} are aspect ratio, airplane efficiency and minimum parasitic drag coefficient. C_{Dmin} is defined by,

$$C_D = C_{D\min} + \frac{C_L^2}{\pi eA} \tag{4}$$

Required thrust curves in Fig.5 consist of function of v^2 as shown in Eq.(3).

Required thrust curves for three types of wings are plotted in Fig.5. The wings of F195 and US147 have Duralumin frames, and that of EXT160 has CFRP frames. 3DTR can have different specifications simply by changing its wing type.[7)]

3. Turbojet Engine of 3DTR

Thrust generation systems with bare propeller blades are not suitable for this kind of robots because of considerably large sizes of hazardous rotational bladed thrusters whose diameters are estimated as about 1350mm for the present 3DTR. Safety is one of the most important features of robots. So, we have chosen turbo jet engines as thrusters for 3DTR.

A modern jet engine has advantages as the following; protection against possible injury, little vibration, space saving, lightweight due to high thrust per weight ratio and reliability. Recent innovation of turbo jet engines has achieved high thrust per weight ratio of up to 6 and is able to reduce thruster weight to 8kg at maximum thrust of 47kgf.

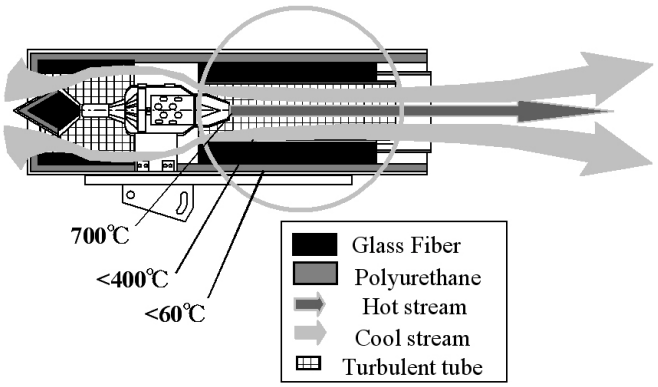

Fig. 6 A silent turbojet engine for 3DTR-II.

However, a turbojet engine has a serious problem of large acoustic emission. We measured a purchased turbojet engine noise and obtain an unbearable noise level of 110dB. So, we have invented a silencer of the turbojet engine. Figure 6 shows the structure of the silent turbojet engine. It has both of high efficient noise reduction system and air-cooling system. The air-cooling system prevents burn accidents from high temperature jet stream.

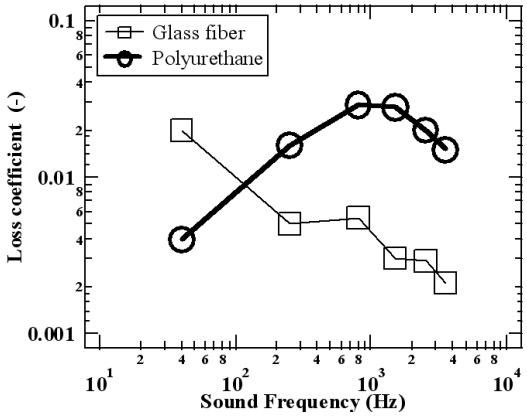

Fig. 7 Efficiency of noise reduction materials.

Figure 7 shows noise reduction effects by two kinds of noise reduction materials applied to 3DTR turbojet engine. Glass fiber and polyurethane reduce respectively low and high frequency band noise emission, and a combination of them realizes highly efficient noise reduction.

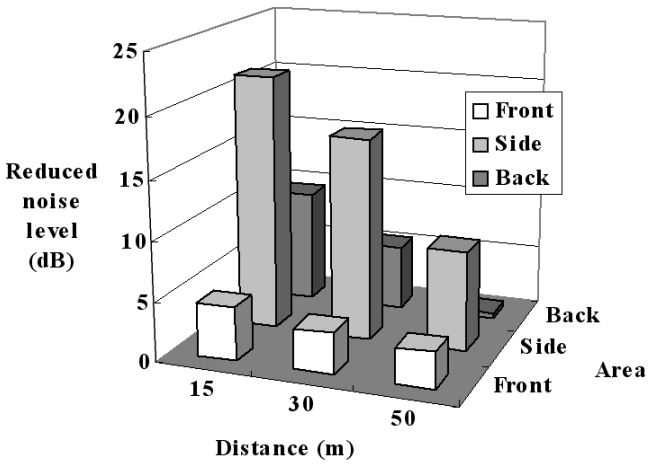

Fig. 8 Effects of noise reduction.

Figure 8 shows summary of noise reduction effects of the silencer system. Reduced noise level in Fig.8 implies a difference between an original and an improved. Noise levels were measured in front, side and back of turbojet engines at distances of 15m, 30m and 50m. Maximum noise reduction of 20dB was obtained at a side of the improved turbojet engine.

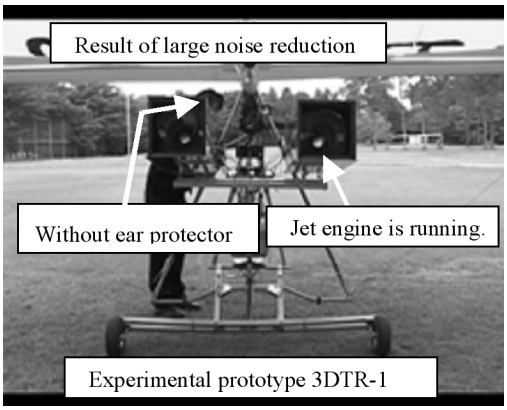

Fig. 9 Running silent jet engines and an operator standing close to them.

Figure 9 is a field test scene of an experimental prototype called 3DTR-I. Two silent jet engines were mounted on 3DTR-I. An operator was able to do his work without ear protectors even very close to the running jet engines.

4. Construction of 3DTR

Construction of 3DTR-I was started in 2004. The purpose of 3DTR-I construction is to obtain design data on the structure, shape, function, physical stability and strength. The construction work was carried out in a repetitive scrap and build manner at an AIST machine shop. In 2005, 3DTR-I was completed and rolled out to a test runway of AIST as shown in Fig.10.

Fig. 10 Taxing of 3DTR-I on a runway.

Figure 11 shows the folded 3DTR-I during parking in a garage. 3DTR-I occupied only less than a half area of an automobile parked nearby as shown in Fig.11. This compactness was realized by the flexible wing concept as shown in Fig.4.

Fig. 11 The folded 3DTR-I can only occupies a small parking surface area.

3DTR-II was then constructed as a flight test model. It has an improved body structure in strength with reinforced suspensions and actuators compared with 3DTR-I. Table 2 shows specifications of 3DTR-II. Large wing area of 18.1m^2 is required to carry a certain mount of payload for small cargo transportation.[4)]

This size of remote piloted airplane are proposed in 1999, [8)] however, it was not for autonomous traffic system with autonomous attitude and tracking control capability.

Figure 12 shows a right-rear view of 3DTR-II. Fuel tanks are located at the center of the dangling body in order to keep its balance during flight. Four Lead-acid batteries are equipped as an energy source for roll- and pitch-actuators and as ballast. The batteries are mounted on a bottom frame bone of 3DTR-II and their large weight of 20kg makes the CG of 3DTR-II lower. 3DTR-II is steered by shifting of its gravity center like a pendulum using the roll- and pitch actuator. A dangling body of 3DTR-II acted as a weight of a pendulum and needs some suitable volume in order to keep good stability. A spread foldable wing is jointed to the dangling body frame through a single point near the center of MAC. The joint between the wing and the dangling body frame of 3DTR-II consists of roll- and pitch-actuators. Twin silent turbojet engines are mounted on the upper dangling body. This thrust point is important to stabilize pitch attitudes of 3DTR-II.

Table.2 Specification of 3DTR-II.

Width	10500mm
Length	3500mm
Height	2500mm
Total weight	95kg
Wheelbase	2000mm
Tread	1800mm
Wheel radius	200mm
Max. engine thrust	230N@108000rpm each
Engine weight	8kg x2 units
Idling rotation	36000rpm
Max. rotation	108000rpm
Engine diameter	320mm
Engine length with silencer	1000mm
Engine response	3.5sec/36000-108000rpm
Actuator: DC motor	48V, 150W x2 units
Battery	12V x 12Ah x4 units

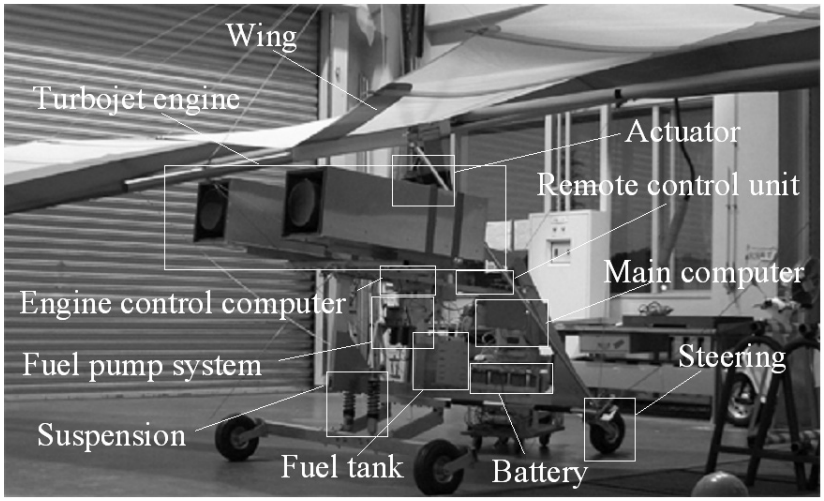

Fig. 12 Right rear view of 3DTR-II.

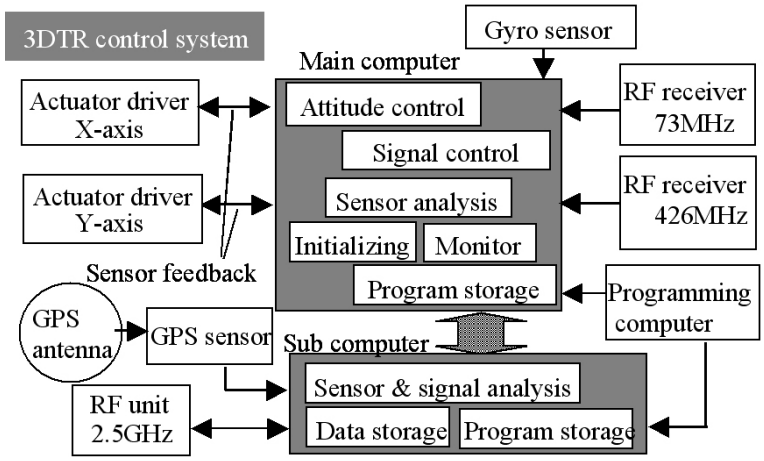

Fig. 13 Control system of 3DTR-II.

A suspension system consisted of twin coils and dumpers are quite effective for landing shock reduction. Dumping rate can be arbitrary chosen depending on runway conditions. Steering of the front wheel is necessary to keep right direction on a runway for take-off. The main computer mounted on the center of the dangling body controls vehicle attitude automatically driving the actuated joint. Commands from the operator are transmit to the main computer through the radio signal receiver as shown in Fig.13.

5. Flight Experiments of 3DTR

Flight experiments were conducted in order to measure take-off speeds and distances and check the corresponding thrusts. On November 22 in 2005, 3DTR-II made its successful first flight. Figure 14 shows a recent scene to minimize ground-run-distance for take-off. We have accomplished the distance reduction up to 36m in 2006. The take-off speed was 32.4km/h (9.0m/s) and the wing attack angle was 16 degrees. The attack angle should be adequately controlled by the pitch-actuator because the angle varies according to turbojet thrust levels, location of CG and airspeed of 3DTR-II.

The measured flight speed of 32.4km/h is slower than the swing arm speed of 40km/h in Fig.2. The technology consisting of slow speed 3DTR and high-speed ground-based manipulation robots are already over rapped at present.[9,10)]

Fig. 14 Flight test of 3DTR-II.

6. Results and Discussion

Usually, An airplane with fixed wing is not able to change its angle of attack (AOA) on the ground because the body and wing are fixed. However, AOA of the 3DTR is variable even on the ground as shown in Fig.15.

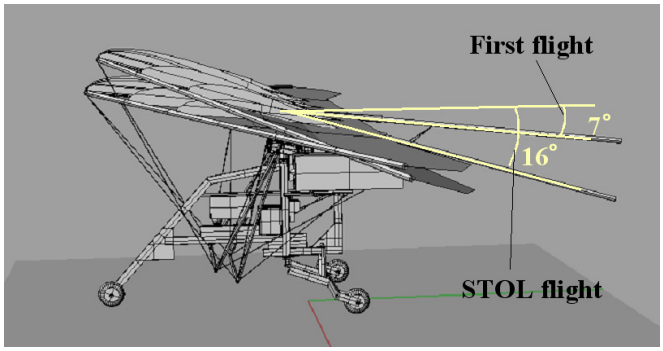

Fig. 15 AOA of 3DTR-II.

So, take-off sequence of 3DTR-II is described by continuous function as shown in Fig.16. Figure 16 indicates the relation of air drag, friction drug between runway and wheels and Jet thrust forces during take-off sequence of 3DTR-II.

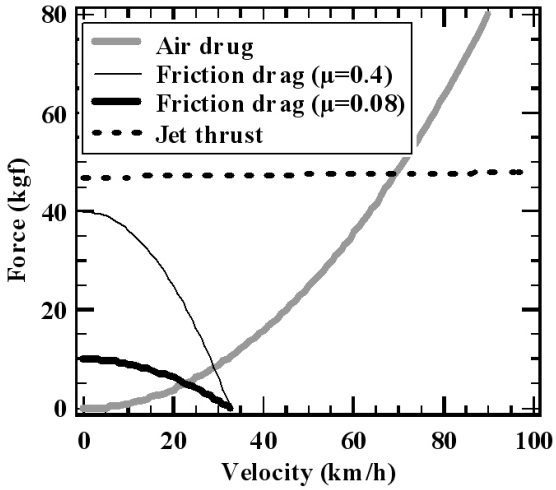

Fig. 16 Force during take-off sequence of 3DTR-II.

Air drag and friction drug in Fig.16 are given as following,

$$D = C_D (1/2)\rho V^2 S \tag{5}$$

$$M = \mu(W - L) = \mu(W - C_L (1/2)\rho V^2 S) \tag{6}$$

Where L:lift, D:drag, T:thrust, W:weight, ρ:air density, V:air speed, S:wing area, C_D:drag coefficient, C_L:lift coefficient, μ:friction coefficient.

Take-off speed is given by Eq(6) when M=0 as following.

$$V = \sqrt{\frac{2W}{\rho C_L S}} \tag{7}$$

C_L is a function of AOA: α. Until stall angle of attack, a sine function approximation of C_L was adapted. Theoretical relation of V vs. ground run distance and V vs. AOA are respectively plotted in Fig.17 and 18.

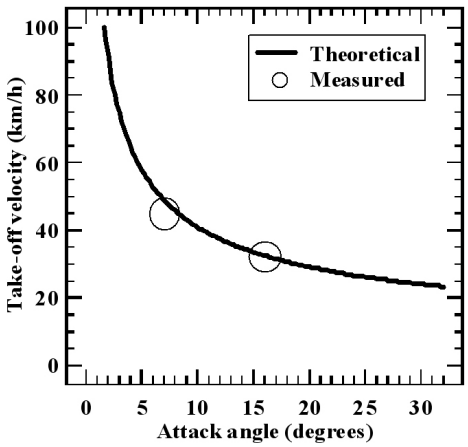

Fig. 17 Take-off velocity of 3DTR-II.

Measured data from flight test are also plotted in Fig.17 and 18.

Theoretical curves of both Fig.17 and 18 are close to measured point. This theory is useful for 3DTR because 3DTR will be able to select AOA automatically depending on length of the runway.

Test flights of 3DTR-II were carried out on the paved runway that has low μ of 0.08 as shown in Fig.16. We are able to calculate the case of rough and grass runway which has high μ of 0.4 and obtain that 3DTR-II is able to take off due to enough power of its jet thruster as shown in Fig.16.

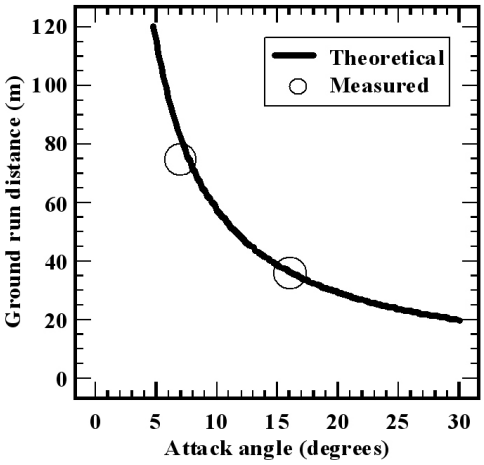

Fig. 18 Ground run distance of 3DTR-II.

Tested 3DTR-II used a F195 type wing as shown in Fig.5. Stoll angle of attack of this F195 type wing is around 30 degrees. Theoretical calculation in Fig.18 indicates that it is able to shorten the ground run distance around 25m. More, we can shorten it to about 10m when we use catapult, and if we lift up the catapult in the air, ground-based manipulation robots for launch 3DTR will appear.

7. Conclusion

A concept and design data for an aerial robotic system for transportation and logistics was proposed, and a basic flight model of 3DTR was successfully constructed as a prototype aerial robot for transportation and logistics. Flight experiments have verified the following features of 3DTR-II;

1) 32km/h as the lowest flight speed,
2) 36m as the shortest take-off ground-run distance,
3) Pendulum stability of attitude in the air,
4) Silent turbojet engines with a newly invented noise reduction system.

The first flight was successfully made on November 22, 2005.

Considerably large commercial markets for personal air transportation will be created in the near future and we firmly believe that highly automated small vehicle for personal use will foster a large industry.

Acknowledgments

The authors would like to express thanks to Dr. M.Onda and Dr. K.Nagai in JAXA for grate contribution in flight test. The authors would like to thank Dr. S.Hirai, Dr. H.Hirukawa and Prof. K. Tanie for useful discussions. This research was partly sponsored the Japan Society for Promotion of Science (JSPS) under Grants-in-Aid for Scientific Research (No.18700203).

References

(1) Amidi, O., Kanade, T., Fujita, K., “A Visual odometer for autonomous helicopter flight.” Robotics and Autonomous Systems, Vol.28, 1999, pp. 185-193.
(2) Helble, H., Cameron, S., “OATS: Oxford Aerial Tracking System.”, Robotics and Autonomous Systems, Vol.55, 2007, pp. 661-666.
(3) Ren, W., “On Constrained Nonlinear Tracking Control of a small Fixed-wing UAV.”, Journal of Intelligent and Robotic Systems, Vol.48, 2005, pp. 525-537.
(4) kurabayashi, D., Noda, K., Asama, H., Kawabata, K., Kaetsu, H., Hashimoto, H., “Information Assistance for Search-and-Rescue by Intelligent Data Carriers and a Data Retrieval Blimp.” Journal of Robotics and Mechatronics, Vol.15, No.5, 2003, pp.521-527.
(5) Iida, F., “Biologically inspired visual odometer for navigation of a flying robot.”, Robotics and Autonomous Systems, Vol.44, 2003, pp. 201-208.
(6) Ollero, A., Merino, L., “Control and perception techniques for aerial robotics.”, Annuak Reviews in Control, Vol.28, 2004, pp. 167-178.
(7) Iwata, K., Maekawa, H., Morikawa, Y., Matsumoto, O., Sarata, S., and Komoriya, K., “Research of 3-dimentional transportation robot (3DTR)(1st Report),” SICE System Integration Division Annual Conference, 1A2-3, SICE, Tsukuba, Japan, 2004, pp. 70-72. (in Japanese Language)
(8) Martinez, R., Hernandez, C., “Preliminary design of a low speed, long endurance remote piloted vehicles (RPV) for civil applications.”, AIRCRAFT DESIGN, Vol.2, 1999,

pp.167-182.
(9) Iwata, K., “Aerial Robotics for Logistics,” JSME News, Vol.18, No.1, June 2007, pp. 4-5.
(10) Iwata, K., Onda, M., and Komoriya, K., "UAV for Small Cargo Transportation", AIAA Infotech Aerospace 2007 Conference and Exhibit, AIAA Meeting Papers On Disc, 9-2784, pp.1-6、June 2007.